Supplementary Information

An isochoric optical platform for interrogation of aqueous glass formation processes

Soheil Kavian[1], Ronald Sellers[1], Carla Berrospe-Rodriguez[1], Crysthal Alvarez[1], Fernanda Velasco[1], Hunter B. Smith[1], Guillermo Aguilar[1,2], Matthew J. Powell-Palm[1,2,3]*

[1]J. Mike Walker '66 Department of Mechanical Engineering, Texas A&M University, College Station, TX,77843, USA
[2]Department of Materials Science & Engineering, Texas A&M University, College Station, TX,77843, USA
[3]Department of Biomedical Engineering, Texas A&M University, College Station, TX,77843, USA

To whom correspondence should be addressed: powellpalm@tamu.edu*

Supplementary Note 1: Thermal Simulation

In order to simulate the heat transfer between the chamber and the solution at different positions, Ansys Fluent was used to better understand temperature changes. For this purpose, 49% DMSO was used as our sample solution for the simulation. We note that this simulation is intended to capture representative scaling of the heat transfer involved in the small-organic-molecule solutions of interest here, as opposed to an accurate estimation of the of the empirical behavior of 49% DSMO specifically.

The primary heat transfer mechanism in the model is conduction. However, the model does not take into account the heat generated due to viscous dissipation. This is because the heat generated by viscous dissipation is insignificant compared to the overall heat transfer process. Hence, the following equation is used for analysis (1):

$$\rho C_p \dot{T} = \nabla.(k\nabla T) \quad (1)$$

In this equation, k represents the thermal conductivity, ρ represents the density of the material, C_p represents the specific heat at constant pressure, and T represents the temperature.

The correlations for density ρ (kg/m3) that are dependent on temperature can be found here (2):

$$\rho = b_2 T^2 + b_1 T + b_0 \quad (2)$$

The relevant constants needed are listed in Table S1.

Table S1. Parameters for the temperature-dependent densities of DMSO solutions of different concentrations (2).

Solution	$b_0 \times 10^{-3}$	$b_1 \times 10$	$b_2 \times 10^3$
7.05 M DMSO	1.090	-6.922	0.257

Experimental DSC data was used to obtain a polynomial correlation for the specific heat [J/(Kg.C)] of 49% DMSO over a temperature range of -150°C to 0°C. The correlation achieved an R^2 value of 0.82.

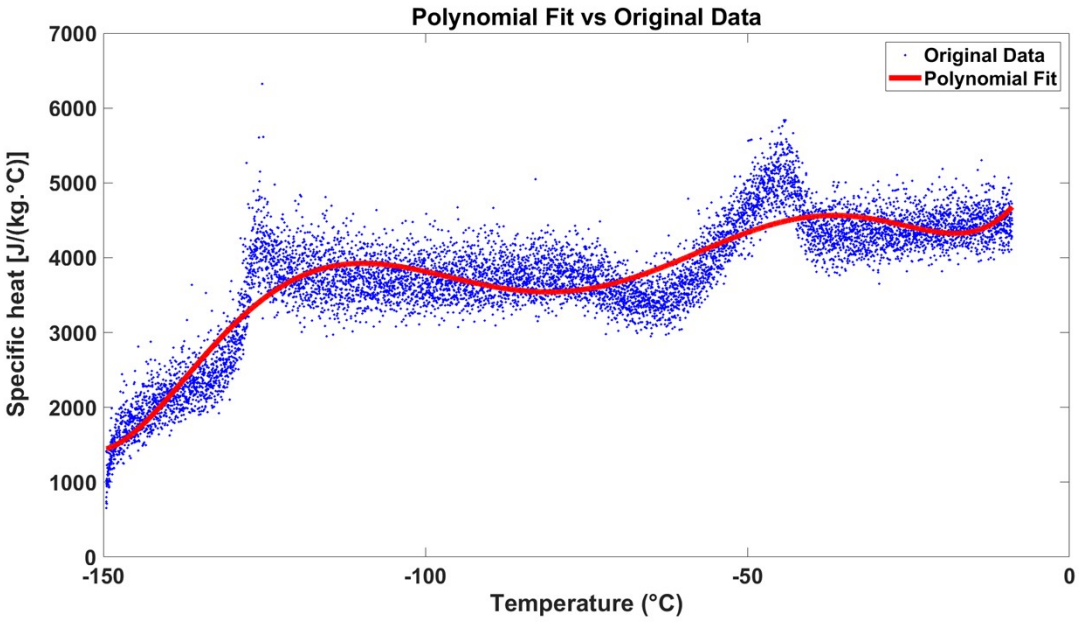

Figure S1. Polynomial-fitted specific heat capacity of 49% DMSO, R^2=0.82 compared to experimental DSC data.

$$C_p \cong C_V = c_1T^6 + c_2T^5 + c_3T^4 + c_4T^3 + c_5T^2 + c_6T + c_7 \quad (3)$$

The obtained coefficients are illustrated in Table S2.

Table S2. Coefficient for specific heat [J/(Kg.C)].

Coefficient of Specific Heat	7.05 M DMSO
c_1	6.42×10^{-8}
c_2	3.05×10^{-5}
c_3	5.48×10^{-3}
c_4	4.64×10^{-1}
c_5	18.78
c_6	336.31
c_7	6478.96

Morover, based on the experimental DSC data, a latent heat of 20536.8 J/kg is obtained for the temperature range between -125°C to -132°C, where the glass transition occurs. This latent heat value is used as an input for simulation.

Thermal conductivity (W/m.K) of DMSO for different temperatures is calculated using the correlation of Ehrlich et al. (3).

$$Thermal\ Conductivity\left(\frac{W}{m}.K\right) = a_1T^4 + a_2T^3 + a_3T^2 + a_4T + a_5 \quad (4)$$

The coefficients can be found in Table S3.

Table S3. Polynomial Approximation of thermal conductivity (3).

Coefficient of Thermal Expansion	**7.05 M DMSO**
a_1	-2.95×10^{-10}
a_2	-6.87×10^{-8}
a_3	-1.29×10^{-6}
a_4	7.42×10^{-4}
a_5	3.56×10^{-1}

Figure S2 displays the cooling and warming temperature over time, and Table 4 shows the rate of cooling and warming in ^{o}C/s and ^{o}C/minute. These measurements were taken for a solution containing 49% DMSO, and the results are comparable to other solutions examined in this study. It is worth noting that the warming temperature serves as a transient boundary condition at the chamber wall to ensure accurate simulation results.

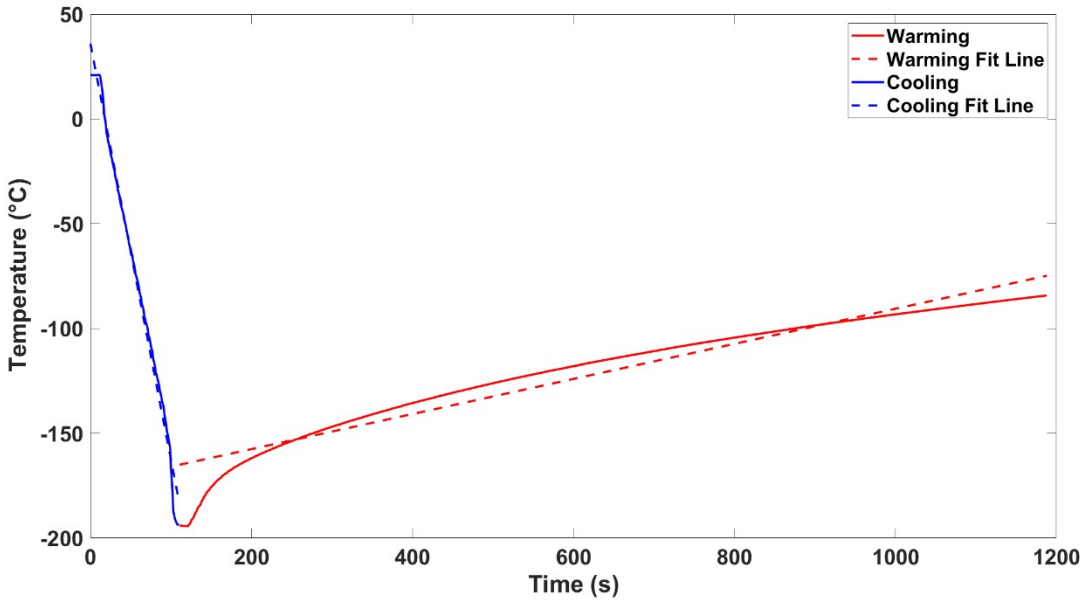

Figure S2. Temperatures of 49% DMSO at different times during cooling in liquid nitrogen and subsequent warming in the environment.

Table S4. the rate of cooling and warming in °C/s and °C/minute.

Unit	Cooling rate	Warming rate
°C/s	3.2790	0.0837
°C/Minute	196.7429	5.0247

Supplementary Note 2: Glass transition detection function

The following are the steps to develop a function in MATLAB to detect the glass transition point based on the average intensity curves obtained by the CLI isovitriscope method or DSC curves:

1. Data Smoothing using LOESS:

   Before processing the data, noise is reduced using the Locally Estimated Scatterplot Smoothing (LOESS) method (4). This method helps in refining the data, making it more suitable for analysis. This can be represented by:

$$y_i^{'} = LOESS(y_i) \tag{5}$$

where y_i are the original data points and $y_i^{'}$ are the smoothed data points.

2. Calculating the Tangent Slopes:

   For each temperature point T_i within a defined range, the function calculates the slopes of lines tangent to the curve at points T_{i-a} to T_{i+a}. This involves computing the first derivative, approximated as follows:

$$f^{'}(Ti) \approx \frac{y_{i+a} - y_{i-a}}{T_{i+a} - T_{i-a}} \tag{6}$$

Here, y_{i+a} and y_{i-a} are the smoothed intensity values at temperatures T_{i+a} and T_{i-a}, respectively. The parameter a a represents the number of steps before and after each temperature point. The choice of a =10 in our study is based on several considerations including the resolution of data, and the balance between accuracy and smoothness. Also, it was found that a=10 is effective in accurately capturing the changes in slope that indicate a glass transition without being overly sensitive to minor fluctuations.

3. Difference of Tangent Slopes:

The function then calculates the differences between the tangent slopes at adjacent points along the temperature axis. This calculation helps identify significant changes in the slope:

$$\Delta f^{'}(Ti) = f^{'}(T_{i+1}) - f^{'}(T_{i-1}) \quad (7)$$

This difference approximates the second derivative, $f''(Ti)$, highlighting inflection points or maximum rate changes in the curve.

4. Identifying the Glass Transition Point**:**

The glass transition point is identified as the temperature at which the difference between subsequent tangent slopes ($\Delta f'(T_i)$) is maximized:

$$T_g = \arg max_{Ti} |\Delta f^{'}(Ti)| \quad (8)$$

This is where the maximum change in the derivative occurs, signifying the glass transition temperature.

Supplementary Note 3: Additional timelapse images

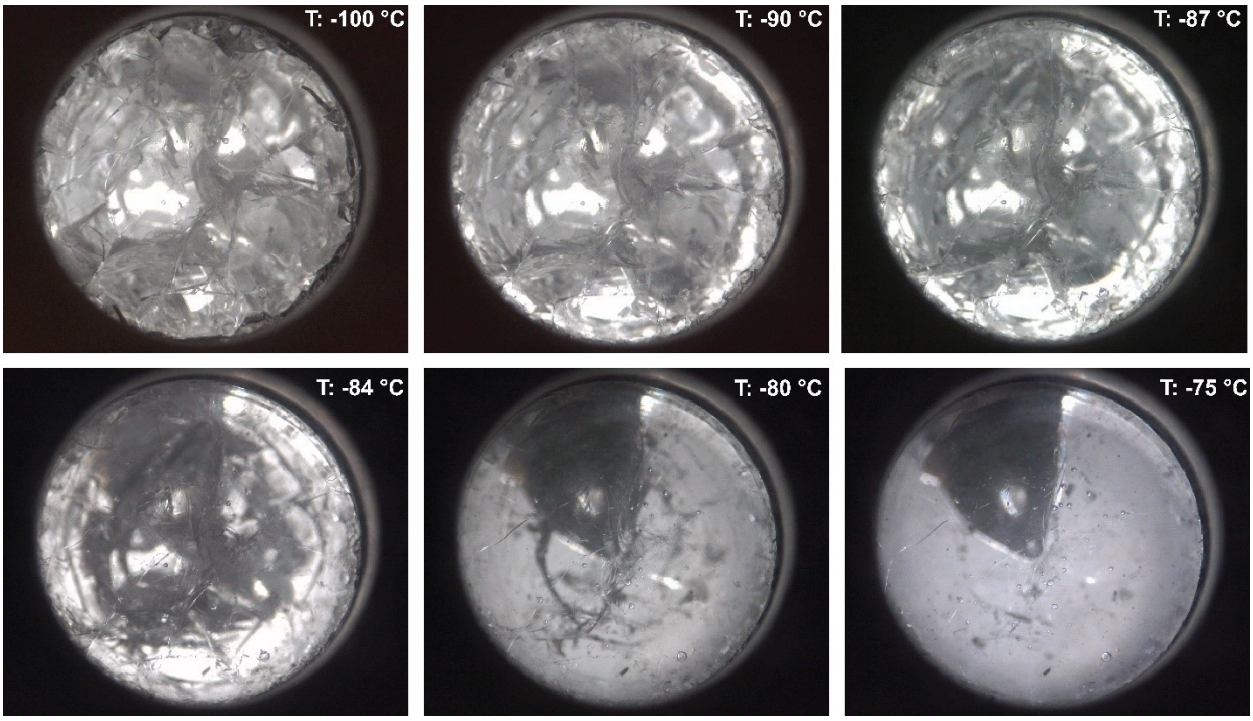

Figure S3 The representative timelapse recorded using DLI monitoring after vitrification at a cooling rate of ~120°C/min, shown in the glass transition temperature range for 79% Glycerol.

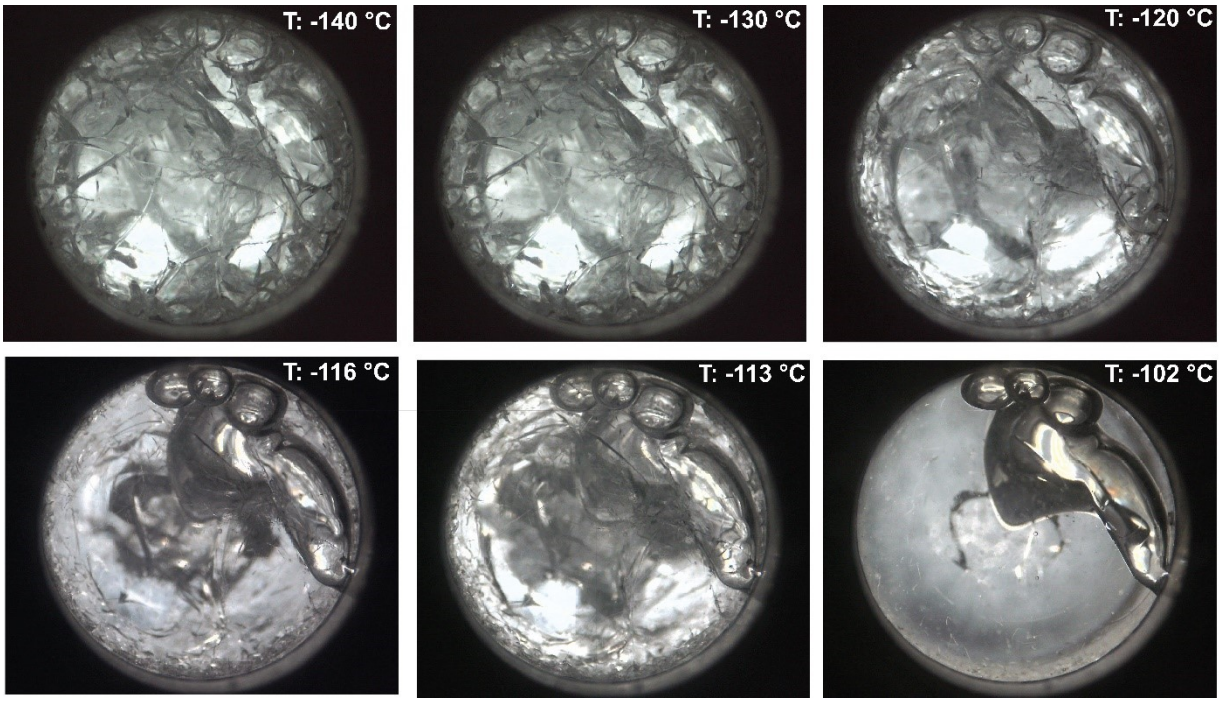

Figure S4 The representative timelapse recorded using DLI monitoring after vitrification at a cooling rate of ~120°C/min, shown in the glass transition temperature range for 59% EG.

Supplementary Note 4: Measured glass transition temperatures

Table S5. Comparison of the measured glass transition temperature through constant light intensity and DSC method with the literature (5-8).

Sample		Isovitriscope T_g (°C)			DSC T_g (°C)			Literature Temp (°C) (5-8)
		Trial 1	Trial 2	Trial 3	Trial 1	Trial 2	Trial 3	
49% DMSO	~5 °C/min cooling rate	-131.35	-131.29	-131.82	-130.96	-129.49	-130.46	-132
	~200 °C/min cooling rate	-129.52	-130.68	-129.07	-	-	-	
59% EG	~5 °C/min	-128.19	-129.18	-130.67	-129.71	-129.29	-129.28	-128

	cooling rate							
	~200 °C/min cooling rate	-128.01	-128.04	-129.83	-	-	-	
79% Glycerol	**~5 °C/min cooling rate**	-101.88	-99.01	-102.66	-103.84	-101.36	-101.39	-101
	~200 °C/min cooling rate	-100.62	-98.06	-100.20	-	-	-	

Supplementary Note 5: Raman measurements

Raman setup

The custom optical system to measure the Raman scattering signal from the ishochoric chamber containg the binary solutions is presented in Figure S.5.1. A continuous wave (C.W) laser at λ=532 nm, with a laser power of 25 mW, was focused into a ~60 μm spot size, using a 10X microscope objective with a focal distance f= 11 mm in the center of the chamber. Both Raman and Rayleigh scattering light where collected and collimated by a lens of f=30 mm and focused to a multimode optical fiber, connected to a VIS-NIR spectrometer (Ocena Insight HR400). A dichroic mirror with a transmision band from 535 to 1200 nm and double notch filter were placed before the optical fiber to reduce as much as possible the Rayleigh scattering from the solution emission. The spectra were colected using OceanView software after removing the background intensity from ambient illumination. The Raman spectrum was recorded with 10 seconds of acquisition time, while 12 measurements were averaged internally with the software.

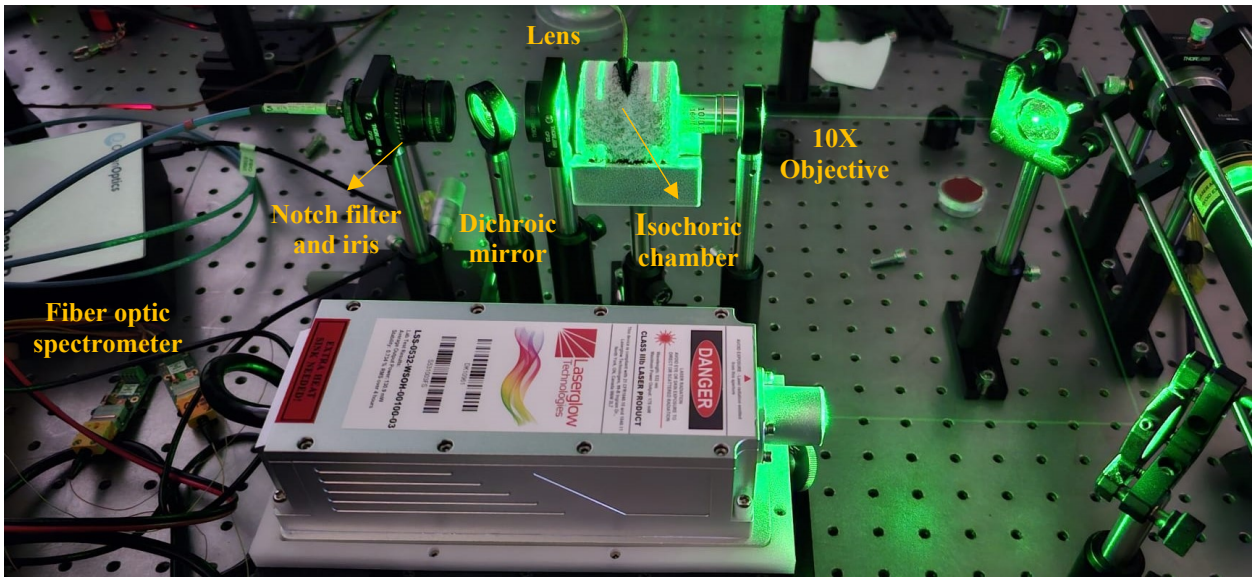

Figure S.5.1 Custom Raman system to study the phenomenology of glass formation and rewarming under isochoric conditions of binary solutions.

Raman spectra of binary solutions

The Raman spectra (from 200 to 4000 cm^{-1}) for 45% DMSO, 79% Glycerol and 59% EG showing the chemical composition at room temperature of these solutions is shown in Figure S.5.2. The spectra show the principal modes that all the solutions have in common (CH_3 bending, CH_3 stretching and OH stretching mode).

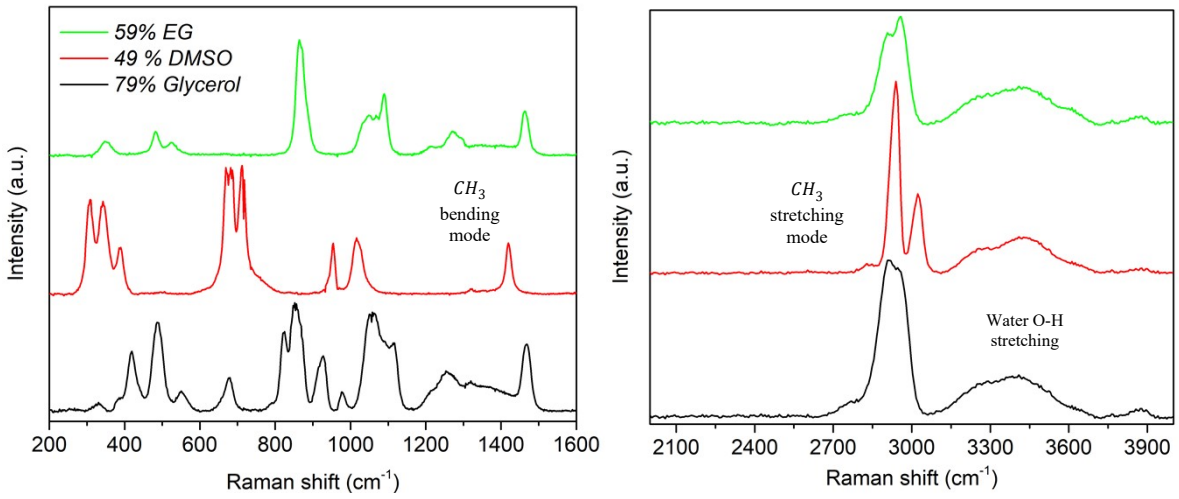

Figure S.5.2 Raman spectra for 45% DMSO, 79% Glycerol and 59% EG.

Supplementary References

1. Holman J. Unsteady-state conduction. Heat transfer. 1997;8:140-217.
2. Solanki PK, Rabin Y. Perspective: temperature-dependent density and thermal expansion of cryoprotective agents. CryoLetters. 2022;43(1):1-9.
3. Ehrlich LE, Feig JS, Schiffres SN, Malen JA, Rabin Y. Large thermal conductivity differences between the crystalline and vitrified states of DMSO with applications to cryopreservation. PLoS One. 2015;10(5):e0125862.
4. James G, Witten D, Hastie T, Tibshirani R. An introduction to statistical learning: Springer; 2013.
5. Shaw JM, Kuleshova L, Macfarlane DR, Trounson AO. Vitrification properties of solutions of ethylene glycol in saline containing PVP, Ficoll, or dextran. Cryobiology. 1997;35(3):219-29.
6. Fahy GM, Wowk B. Principles of cryopreservation by vitrification. Cryopreservation and freeze-drying protocols. 2015:21-82.
7. Rasmussen D, MacKenzie A. Phase diagram for the system water–dimethylsulphoxide. Nature. 1968;220(5174):1315-7.
8. Zamecnik J, Faltus M, Bilavcik A. Vitrification solutions for plant cryopreservation: Modification and properties. Plants. 2021;10(12):2623.